



HAL
open science

Unveiling the Ir single atoms as selective active species for the partial hydrogenation of butadiene by operando XAS

W. Liu, F. Morfin, K. Provost, M. Bahri, W. Baaziz, O. Ersen, L. Piccolo, C. Zlotea

► To cite this version:

W. Liu, F. Morfin, K. Provost, M. Bahri, W. Baaziz, et al.. Unveiling the Ir single atoms as selective active species for the partial hydrogenation of butadiene by operando XAS. *Nanoscale*, 2022, 14 (20), pp.7641-7649. 10.1039/d2nr00994c . hal-03682084

HAL Id: hal-03682084

<https://hal.science/hal-03682084v1>

Submitted on 12 Oct 2022

HAL is a multi-disciplinary open access archive for the deposit and dissemination of scientific research documents, whether they are published or not. The documents may come from teaching and research institutions in France or abroad, or from public or private research centers.

L'archive ouverte pluridisciplinaire **HAL**, est destinée au dépôt et à la diffusion de documents scientifiques de niveau recherche, publiés ou non, émanant des établissements d'enseignement et de recherche français ou étrangers, des laboratoires publics ou privés.



HAL
open science

Unveiling the Ir single atoms as selective active species for the partial hydrogenation of butadiene by operando XAS

W. Liu, F. Morfin, K. Provost, M. Bahri, W. Baaziz, O. Ersen, L. Piccolo, Claudia Zlotea

► **To cite this version:**

W. Liu, F. Morfin, K. Provost, M. Bahri, W. Baaziz, et al.. Unveiling the Ir single atoms as selective active species for the partial hydrogenation of butadiene by operando XAS. *Nanoscale*, Royal Society of Chemistry, 2022, 14 (20), pp.7641-7649. 10.1039/d2nr00994c . hal-03679755

HAL Id: hal-03679755

<https://hal.archives-ouvertes.fr/hal-03679755>

Submitted on 27 May 2022

HAL is a multi-disciplinary open access archive for the deposit and dissemination of scientific research documents, whether they are published or not. The documents may come from teaching and research institutions in France or abroad, or from public or private research centers.

L'archive ouverte pluridisciplinaire **HAL**, est destinée au dépôt et à la diffusion de documents scientifiques de niveau recherche, publiés ou non, émanant des établissements d'enseignement et de recherche français ou étrangers, des laboratoires publics ou privés.

Unveiling the Ir single atoms as selective active species for the partial hydrogenation of butadiene by *operando* XAS

W. Liu¹, F. Morfin², K. Provost¹, M. Bahri³, W. Baaziz³, O. Ersen³, L. Piccolo², C. Zlotea^{1*}

¹ *Université Paris Est, Institut de Chimie et des Matériaux Paris-Est (UMR7182), CNRS, UPEC, 2-8 rue Henri Dunant, 94320 Thiais, France*

² *Univ Lyon, Université Claude Bernard - Lyon 1, CNRS, IRCELYON - UMR 5256, 2 Avenue Albert Einstein, F-69626 Villeurbanne CEDEX, France*

³ *Université de Strasbourg, Institut de Physique et Chimie des Matériaux de Strasbourg (UMR7504), 23 rue du Loess, BP 34 67034 Strasbourg Cedex 2, France*

* Corresponding author email: Claudia.zlotea@cnsr.fr

Abstract

Single-atom catalysts represent an intense topic of research due to their interesting catalytic properties for a wide range of reactions. Clarifying the nature of the active sites of single-atom catalysts under realistic working conditions is of paramount importance for the design of performant materials. We have prepared an Ir single-atoms catalyst supported on a nitrogen-rich carbon substrate that proven a substantial activity toward hydrogenation of butadiene with nearly 100% selectivity to butenes even at full conversion. We evidence here, by quantitative *operando* X-ray absorption spectroscopy, that the initial Ir single atoms are coordinated with four light atoms *i.e.*, Ir- X_4 ($X = C/N/O$) with an oxidation state of +3.2. During the pre-treatment under hydrogen flow at 250 °C the Ir atoms loses one neighbour (possibly oxygen) and partially reduces to an oxidation state around +2.0. We clearly demonstrate that Ir- X_3 ($X = C/N/O$) are the active species with very good stability under reactive conditions. Moreover, Ir single atoms remain isolated under reducing atmosphere at a temperature as high as 400 °C.

Keywords: Ir-single atom catalyst, *operando* XAS, butadiene partial hydrogenation, EXAFS, XANES

1. Introduction

Heterogeneous catalysis is the most important industrial process for producing large-scale chemicals and energy products nowadays. However, the design of catalysts with high efficiency, selectivity and stability remains a major challenge.^{1,2} Recently, single-atom catalysts (SACs), which contain isolated atoms dispersed on a support, have gained considerable attention due to their maximized atomic utilization and unique electronic properties.³⁻⁸ Because of the changes in the active-site structure in comparison with metal nanoparticles or nanoclusters, SACs are expected to have distinct behaviours in catalysis, such as high selectivity and stability.⁹⁻¹¹ Since the first practical report of SACs (Pt/FeO_x) by Qiao *et al.*¹² in 2011, significant progress has been made in this field.¹³⁻¹⁶ SACs have shown superior catalytic performance (activity and/or selectivity) for several industrial relevant reactions.¹⁷⁻¹⁹

Selective hydrogenation reactions play a key role in the field of sustainable chemistry. The over-hydrogenation of the desired product remains a major issue for these reactions.²⁰ Among them, refining of C₄ cuts from steam cracking by catalytic selective hydrogenation is an important industrial process. Butene products, 1-butene and 2-butenes, are intermediates used in industry for polymerization and alkylation processes, respectively.²¹⁻²³ The presence of 1,3-butadiene (0.3% to 6%) in C₄ species is considered as a poison which causes unwanted side reactions and deactivates the catalysts.²⁴ Commonly, catalysts based on Pd and Pt are widely used due to their high activity²⁵⁻²⁹ but their selectivity to butene is limited at high butadiene conversion.³⁰

Over the last few years, researchers have reported the selective hydrogenation of 1,3-butadiene on SACs which showed promising catalytic performance. For example, Lucci *et al.*³¹ reported that low concentration Pt single atoms supported on a Cu surface showed 90% selectivity to butenes at full conversion and the catalyst remained stable over 2 days at 160 °C. Through a DFT study, Lv *et al.*³² showed that Pt single atoms adsorbed on Cu surface [Pt₁/Cu(1 1 1)] has a higher selectivity toward 1-butene than a clustered Pt-content catalyst [Pt_{4-line}/Cu(1 1 1)]. Yan *et al.*³³ compared an atomically dispersed Pd₁/graphene catalyst with 3 different Pd carbon-supported nanocatalysts. The SAC showed a high activity by retaining 100% butenes selectivity up to 95 % conversion while the selectivity of Pd nanocatalysts dropped sharply at high 1,3-butadiene conversion. Furthermore, Zhang *et al.*³⁴ found that a very low concentration (0.08

wt.%) of isolated Au³⁺ on a ZrO₂ support is highly selective in the hydrogenation of 1,3-butadiene to butene isomers. However, Ir single atom catalysts have never been reported for this reaction.

A fine description of the active species of single-atom catalysts and their local and electronic structures are very scarcely identified, whatever the reaction targeted. Only very recently, Fang *et al.*³⁵ proposed the evolution of Pt single-atoms into a near-free state as active species in the electrocatalytic hydrogen evolution reaction. They revealed that during the reaction, the single Pt atom tends to dynamically release from the nitrogen-carbon substrate, with the structure less coordinated to the support and the electronic properties close to zero valence.

In this work, we report the synthesis and characterization of Ir single-atoms dispersed on a nitrogen-rich carbon substrate and their catalytic activity for the partial hydrogenation of butadiene. To reveal the active species of the Ir SAC and their local and electronic structures under working conditions, we have carried out *operando* XAS experiments. For the sake of comparison, Ir nanocatalysts have been also investigated under the same conditions.

2. Experimental methods

2.1. Catalyst preparation

We have prepared Ir single-atom catalyst (Ir-SAC) supported on a nitrogen-doped carbon starting from a commercial porous activated carbon (AC with a specific surface area of 1400 m²/g purchased from STREM Chemicals) as initial substrate. The initial AC contains small amount of impurities, mainly aluminosilicates, that are noticeable in the XRD patterns as sharp peaks. The Ir-SAC was prepared by a cascade anchoring strategy adapted from Zhao *et al.*³⁶ The Ir atoms were dispersed on a activated carbon in a nitrogen-rich carbonaceous medium by the liquid impregnation of the pristine AC with IrCl₃·xH₂O precursor in aqueous solution in the presence of a chelating agent (ethylenediaminetetraacetic acid: EDTA) and a source of nitrogen (melamine) followed by pyrolysis under Ar flow at 800 °C.

For the sake of comparison, we have prepared Ir nanocatalysts (Ir-NC) in the form of well dispersed nanoparticles by a simple method based on the liquid-phase impregnation of the same AC support with the IrCl₃·xH₂O precursor in aqueous solution, followed by reduction under 5%H₂/Ar flow at 800 °C, as described earlier.³⁷

Synthesis of Ir-SAC

First, 400 mg of EDTA (Sigma-Aldrich), used here as chelating agent, was dispersed in 10 mL distilled water and $\text{NH}_3 \cdot \text{H}_2\text{O}$ was added to adjust the solution p-H to dissolve the EDTA. Then, 0.0213 mmol of $\text{IrCl}_3 \cdot x\text{H}_2\text{O}$ (Alfa Aesar) and 200 mg of AC were added to the solution and the mixture was stirred and evaporated at 60 °C. The metal ions are thus chelated by EDTA then anchored onto the carbon support by solvent evaporation. Moreover, the excessive chelating agent bound to the support surface will physically isolate the metal complex. The recovered solid was dried at 70 °C overnight. During the second step, the dried carbon-based powder was hand ground with 1000 mg of melamine (Sigma-Aldrich), as a nitrogen source for the subsequent step. The final stage of the synthesis consists in the pyrolysis of the obtained mixture at 800 °C under Ar flow for 2 h in a furnace (ramp 3 °C/min, 200 mL/min). During this step, the chelated metal complex can react with carbon nitrogen species CN_x (such as C_3N_4 etc.) decomposed from melamine at high temperature (> 600 °C) and subsequently metal- N_x moieties are formed, thus preventing metal atoms from aggregation. The Ir single atoms are finally anchored in a nitrogen-rich carbon substrate. The as-prepared Ir-SAC powder was recovered and used without any further treatment.

The elemental analysis of the Ir-SAC sample was determined by ICP-OES and CHNS techniques. The metal amount is 1.0 wt.% for Ir-SAC, while N concentration reaches 14.1 wt.% after the synthesis which is higher than 0.5 wt.% found in the initial AC. Additional results from the elemental analysis of the as-prepared samples are shown in table SI1.

Synthesis of Ir-NC

For the Ir nanocatalyst preparation, 300 mg of AC and 0.065 mmol of $\text{IrCl}_3 \cdot x\text{H}_2\text{O}$ were dispersed in 10 mL distilled water and the solution was stirred and evaporated at 60 °C. The mixture was then dried at 70 °C overnight. The dried powder was reduced under 5% H_2/Ar (0.5 L/min) at 800 °C for 2 h. The as-prepared powder material was further used without any treatment. The metal amount is 3.7 wt.% for Ir-NC, as determined by ICP-OES.

2.2. Physicochemical characterizations

The structural properties of the samples were characterized by powder X-ray diffraction (XRD) using a D8 Advance Bruker diffractometer (Cu K_{α} radiation $\lambda = 1.5406 \text{ \AA}$, Bragg-Brentano geometry).

The samples were characterized by Transmission Electron Microscopy (TEM) with a 200 kV FEG microscope (FEI Tecnai F20 equipped with a Gatan Energy Imaging Filter, resolution 0.24 nm). A small amount of sample was ultrasonicated in ethanol solvent, then small drops of suspension were placed on carbon grids. The Ir nanoparticles size distribution and the average size were determined by statistical analyses of several TEM images.

The Ir-SAC specimen was analysed by high-angle annular dark-field imaging in scanning transmission electron microscopy (HAADF-STEM) using a probe corrected JEOL 2100F electron microscope operating at 200 kV. This imaging technique was used to characterize the as-prepared Ir-SAC sample as well as to assess the single atoms stability against coalescence after treatment at high temperature. The thermal treatments were carried out by heating the sample at 250 °C and 400 °C with 10°C/min under 5% H_2 /Ar flow (200 ml/min) in an external resistive furnace.

2.3. Catalytic test

The hydrogenation of 1,3-butadiene on Ir-SAC and Ir-NC samples was carried out under atmospheric pressure in a continuous flow fixed-bed stainless steel reactor. The reactor was placed in a ceramic furnace with temperature control. The temperature of the catalyst was recorded *via* a thermocouple inserted in the catalytic bed. Before the reaction, 40 mg of catalyst was mixed with 100 mg of α - Al_2O_3 (8 m^2/g , purity 99.95% from Alfa-Aesar) and activated *in situ* with hydrogen (70 ml/min) by heating from room temperature to 250 °C at a heating rate of 4 °C/min and remained at 250 °C for 1 h. Then the reactor was cooled down to 25 °C under H_2 . The feed flow rate was set to 100 ml/min. The reactive gases ($C_2H_2:H_2:He$) were mixed using mass flow controllers (Brooks and Vögtlin) with a composition of 2:10:88%. The temperature was heated to 200 °C with a ramp of 1 °C/min and remained at 200 °C for 20 minutes under reactive mixture. The feed and effluent gases were analysed online using Shimadzu GC-2014 gas chromatograph equipped with a Supelco alumina sulphate plot coupled with an FID detector.

2.4. Operando XAS

To check the local and electronic structures of Ir-SAC and Ir-NC samples during the hydrogenation of butadiene, operando X-ray absorption spectroscopy (XAS) experiments coupled with mass spectroscopy were carried on the ROCK beam line³⁸ at the SOLEIL synchrotron. The X-ray absorption spectra at the L₃ edge of Ir (11.215 eV) were measured and metal Ir foil was used as reference. The powder samples were placed inside a Lytle-type cell, which was connected to a gas distribution system that controls the gas flow composition at atmospheric pressure. The experiment followed as close as possible the laboratory reaction conditions. Prior to each experiment, the samples were pre-treated to remove contaminants at the surface by heating to 250 °C (4 °C/min) under continuous H₂/He flow (15 ml/min H₂ and 15 ml/min He) followed by a dwell at 250 °C for 1 h and then cooled down to 25 °C. Afterward, the catalysts were exposed to the reactive gas mixture (35 mL/min): 0.5% C₄H₆ + 2.5% H₂ + 97% He and the temperature was raised to 200 °C with a ramp of 1 °C/min. The temperature was maintained at 200 °C for 1 h under reaction conditions. The XAS measurements were coupled with continuous mass spectrometry (MS) to identify the reaction products.

All XANES spectra were calibrated in energy and normalized. The XAS data treatment and EXAFS refinement were performed with the MAX program package ($E_0 = 11215$ eV for Ir L₃ edge, Fourier Transform 4-15 Å⁻¹).^{39,40} EXAFS fitting was performed on the first sphere filtered spectra. Theoretical phases and amplitudes were computed with FEFF8 based on Ir-X₄ structure. The refined parameters are the coordination number (N), the Debye-Waller factor (σ^2) and the nearest neighbour distance (R). The energy shift ΔE_0 was first refined for the Ir reference and then fixed for the subsequent refinements. The goodness of fit was evaluated using the quality factor (QF).

3. Results and discussions

XRD patterns of the as-prepared Ir-SAC and Ir-NC samples showed only the contribution from the starting activated carbon (AC) support, as shown in Figure 1A. Moreover, no diffraction peaks from the face centred cubic (fcc) lattice of bulk Ir metal were observed in both samples. This suggests that Ir is well dispersed on the carbon host either as small clusters/nanoparticles with too short coherence length to diffract X-rays⁴¹ or as single atoms.

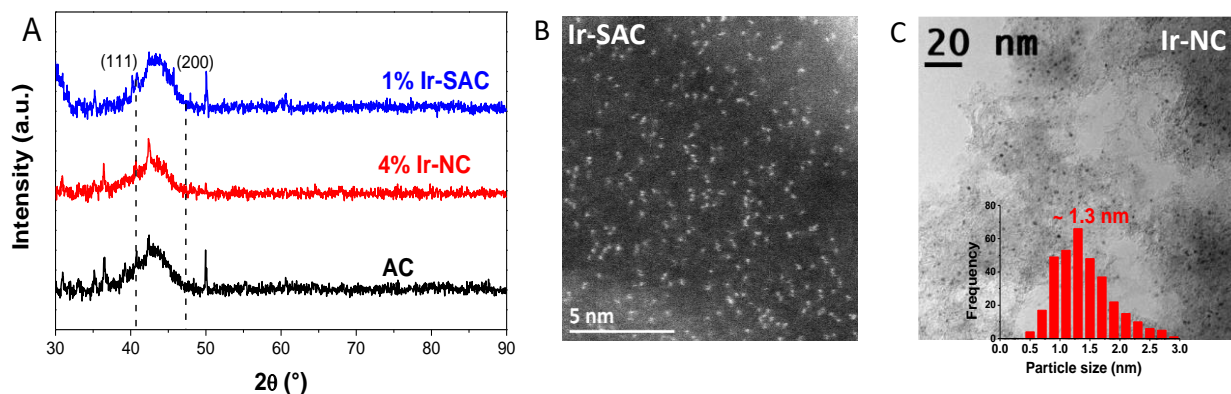


Figure 1. (A) XRD patterns of the starting activated carbon (AC) support together with the as-prepared Ir-SAC and Ir-NC samples; The angular positions of the expected diffraction peaks (111) and (200) of fcc bulk Ir metal are indicated by dashed lines. (B) HAADF-STEM image of Ir-SAC and (C) TEM image of Ir-NC with an average size of 1.3 nm (size histogram in inset).

To check the dispersion of Ir in both as-prepared samples, TEM/STEM characterizations were carried out (Figures 1B and 1C). HAADF-STEM images of the Ir-SAC sample clearly shows isolated bright spots homogeneously dispersed on the support (figure 1B). We hypothesize that these spots are Ir single atoms, as this will be confirmed later by XAS. In the light of the above XRD and STEM-HAADF investigations and the chemical properties of the as-prepared Ir-SAC (1.0 wt.% of Ir and ~ 14 wt.% of N), this sample consists of Ir single-atoms on a nitrogen-rich carbon substrate, as also proposed by Zhao *et al.*³⁶

On the contrary, Ir nanoparticles can be clearly visualized on the carbon support for the Ir-NC sample (Figure 1C). The mean size of Ir nanoparticles is 1.3 (± 0.5) nm, in agreement with the literature for similar synthetic conditions.⁴² Additional HAADF-STEM and TEM images for the as-prepared samples are shown in figure S11.

The conversion and selectivity of Ir-SAC and Ir-NC during the hydrogenation of butadiene reaction are shown in Figure 2. Butadiene conversion is slightly higher for Ir-NC, however Ir-SAC shows an impressive nearly 100% selectivity to butenes in the whole temperature range (25–200 °C). The conversion increases steadily with the temperature and reaches 80% at 200 °C. Ir-NC behaves differently with high selectivity at low temperature and low conversion (below 30%). However, when the conversion exceeds 30% a sudden drop of the selectivity occurs to almost full hydrogenation to butane at high temperature.

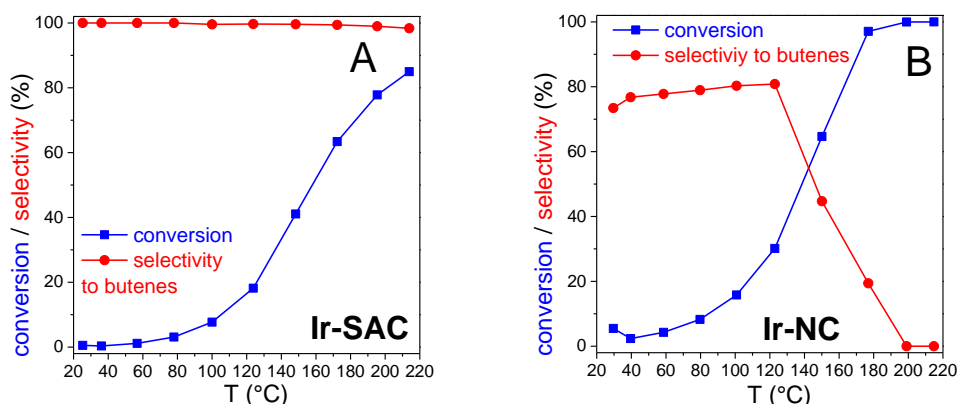


Figure 2. Conversion and selectivity to butenes of Ir-SAC (A) and Ir-NC (B) in the hydrogenation of butadiene as a function of temperature.

To gain insights into the local structure and the electronic features of Ir-SAC and their evolution in reactive conditions, we have performed *operando* XAS experiments at the Ir L₃-edge. The normalized X-ray absorption near edge structure (XANES) spectra and the Fourier Transform (FT) modulus of the k²-weighed extended X-ray absorption fine structure (EXAFS) signal of the Ir-SAC and Ir-NC samples under H₂/He gas mixture at room temperature and prior to the pre-treatment and reaction are shown in Figure 3. For comparison, Ir bulk and IrO₂ references are also plotted.

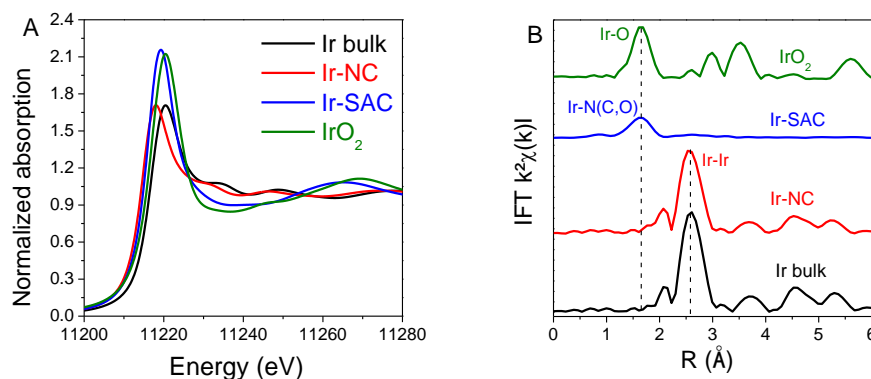


Figure 3. XANES spectra at the Ir L_{3} -edge of the Ir-SAC (blue) and Ir-NC (red) under H_2/He gas flow at room temperature prior to the pre-treatment together with the references: Ir bulk metal (black) and IrO_2 powder (green) (A) and the modulus of the Fourier transforms of the k^2 -weighted EXAFS signals of Ir powder (black), Ir-NC (red), Ir-SAC (blue) and IrO_2 powder (green) (B). Fourier transforms have been stacked for comparison.

As shown in Figure 3A, the Ir L_{3} -edge XANES spectra are characterized by a white line, which corresponds to transitions from the occupied $2p_{3/2}$ core electron level to empty $5d$ states, thus probing the local density of unoccupied final states in the system.⁴³ It is obvious from Figure 3 that the white line of Ir-SAC is comparable to that of IrO_2 and more intense than the one of Ir-NC. The white line of the latter catalyst is close to the one of Ir bulk metal. The increase of the intensity of the white line from Ir-NC to Ir-SAC indicates a larger unoccupancy of $5d$ states in the Ir-SAC which can be explained by the hybridization between Ir and C/N/O atoms from the support.

The above-mentioned white line features can be also understood in terms of oxidation state of the catalyst. The XANES spectra can be exploited to determine the oxidation state more precisely. Hambley *et. al* proposed a simple mathematical method to calculate the oxidation state

using the following equation⁴⁴: $OS_{sample} = \left[\left(\frac{a}{b} \right)_{sample} - \left(\frac{a}{b} \right)_{Ir\ bulk} \right] / \left[\left(\frac{a}{b} \right)_{IrO_2} - \left(\frac{a}{b} \right)_{Ir\ bulk} \right] \times 4$,

where a is the intensity of the white line and b is the gap of the adsorption spectra as shown in Figure S12. Thus, the oxidation state of Ir in Ir-SAC and Ir-NC were calculated accordingly and compared to those of well-known references: 0 and +4 for Ir metal and IrO_2 , respectively (Figure S12).

Consequently, Ir has an oxidation state of $+3.2(\pm 0.1)$ in Ir-SAC, while this value is close to 0 in Ir-NC *i.e.*, comparable to Ir bulk sample. The FT modulus of the k^2 -weighted EXAFS signals of the as-prepared samples are compared to those of bulk Ir and IrO₂ references in Figure 3B. Ir bulk shows typical peaks of the fcc metal with the dominant one at approximately 2.58 Å (Ir-Ir nearest distances) whereas, IrO₂ displays a main peak at around 1.62 Å corresponding to the Ir-O nearest neighbours of the tetragonal structure of the oxide, in good agreement with previous results⁴⁵. The FT modulus of the k^2 -weighted EXAFS signal of Ir-SAC is clearly different as compared to those of the metal and oxide references and features a single peak at around 1.6 Å with low intensity. This unique and less intense peak can be ascribed to the backscattering from the nearest Ir neighbouring light elements such as, N, C or O. However, EXAFS cannot distinguish between light elements close to each other such as, C, N or O because of their similar scattering amplitudes. Nevertheless, it is worth noting that no Ir-Ir scattering peak (around 2.6 Å) is visible in the as-prepared Ir-SAC sample, which clearly confirms the atomic dispersion of Ir, in good agreement with HAADF-STEM investigations (Figure 1B).

The XANES spectra of Ir-SAC during the pre-treatment at 250 °C (under H₂/He flow) and under operando conditions at 200 °C (under reactive gas mixture) are illustrated in Figure 4A and B, respectively. The intensity of the white line smoothly decreases during the pre-treatment heating and stabilizes when reaching 250 °C (Figure 4A). Under reactive conditions, only a very slight variation of the white line intensity can be noticed with increasing and stabilisation of the temperature at 200 °C (Figure 4B). To monitor the change of the electronic properties during pre-treatment and under *operando* conditions we applied Humbley's approach for all XANES data and the calculated oxidation of state is given in Table 1.

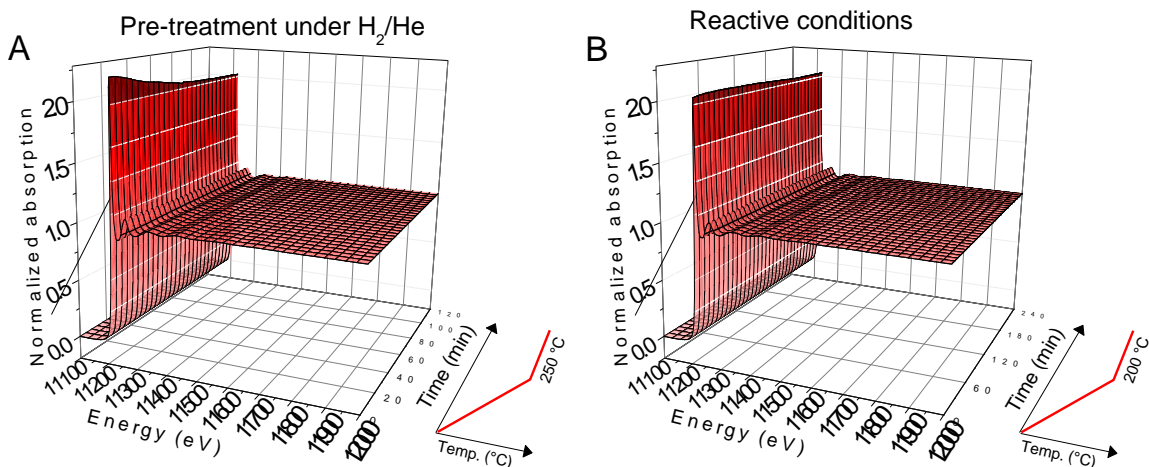


Figure 4. XANES spectra at the Ir L_3 -edge of the Ir-SAC during (A) the pre-treatment under H_2/He flow and (B) under operando conditions.

To reveal the local structure of Ir-SAC during pre-treatment and under reactive conditions, we performed EXAFS refinements based on a structural model where iridium atom is coordinated to four in-plane light atoms $Ir-N_xC_yO_z$ ($x + y + z = 4$), as previously proposed in the literature.^{46,47} The EXAFS fitting results such as, the coordination number (N), the Debye-Waller factor (σ^2) and the nearest neighbour Ir-X distance (R) are listed in Table 1. Typical refinements results are plotted in Figure S13.

The evolution of the coordination number, the nearest neighbour R_{Ir-X} distance and the oxidation state during hydrogenation of butadiene are plotted in Figure 5. It is obvious that the pre-treatment under H_2/He gas mixture at 250 °C strongly affects the single-atom catalyst state whereas only minor changes can be observed under reactive conditions. Therefore, the following discussion will firstly focus on the initial state and the pre-treatment effect on the Ir-SAC and secondly on the catalyst under working conditions.

Conditions			EXAFS				XANES
Step	Gas	T (°C)	N	σ^2 (Å ²)	R (Å)	QF	OS
Initial state	air	25	4.0 (1)	0.0052 (3)	2.016 (1)	0.14	3.2
Initial state	He	25	4.0 (1)	0.0052 (3)	2.016 (1)	0.11	3.2
Introduction of reduction gas	H ₂ /He	25	4.0 (1)	0.0052 (3)	2.016 (2)	0.12	3.2
Pre-treatment ramp	H ₂ /He	25	4.0 (1)	0.0053 (3)	2.016 (1)	0.10	3.2
		50.5	4.0 (1)	0.0055 (3)	2.015 (2)	0.10	3.1
		84.2	3.9 (1)	0.0061 (4)	2.012 (1)	0.07	2.9
		117.6	3.6 (1)	0.0059 (4)	2.008 (1)	0.06	2.6
		150.6	3.3 (1)	0.0059 (4)	2.005 (1)	0.06	2.4
		183.6	3.2 (1)	0.0059 (4)	2.001 (1)	0.05	2.4
		216.3	3.1 (1)	0.0057 (4)	1.999 (1)	0.04	2.1
		252	3.0 (1)	0.0057 (5)	1.997 (1)	0.05	2.0
Pre-treatment at 250 °C	H ₂ /He	250	2.9 (1)	0.0057 (5)	1.996 (1)	0.05	2.0
		250	2.9 (1)	0.0056 (4)	1.995 (1)	0.04	1.9
		250	2.9 (1)	0.0052 (5)	1.995 (1)	0.05	1.9
		250	2.9 (1)	0.0053 (4)	1.995 (1)	0.05	1.8
		250	2.8 (1)	0.0052 (4)	1.995 (1)	0.04	1.8
Pre-treatment cooling	H ₂ /He	34.1	2.9 (1)	0.0049 (4)	1.996 (1)	0.06	1.9
Introduction of reactive gas mixture	C ₄ H ₆ /H ₂ /He	24.9	3.0 (1)	0.0049 (5)	1.997 (1)	0.06	2.0
Reaction ramp	C ₄ H ₆ /H ₂ /He	24.8	3 (1)	0.0048 (4)	1.998 (1)	0.05	2.0
		64.7	3.1 (1)	0.0051 (5)	2.001 (1)	0.06	2.1
		106.5	3.1 (1)	0.0053 (4)	2.001 (1)	0.05	2.1
		147.7	3.1 (1)	0.0054 (4)	1.999 (1)	0.05	2.0
		198.6	3.0 (1)	0.0055 (4)	1.996 (1)	0.05	1.9
Reaction at 200 °C	C ₄ H ₆ /H ₂ /He	200	3.0 (1)	0.0054 (4)	1.996 (1)	0.05	1.9
		200	2.9 (1)	0.0051 (5)	1.997 (1)	0.06	1.9
		200	3.0 (1)	0.0053 (4)	1.996 (1)	0.05	1.9
Final state	He	33.4	3.1 (1)	0.0053 (4)	1.996 (1)	0.05	2.0

Table 1. EXAFS refinements result for Ir-SAC under operando conditions (hydrogenation of butadiene) : the coordination number (N), the Debye–Waller factor (σ^2), the nearest Ir–X (X = N,C,O) distance (R) and the quality of the fit (QF). The values of oxidation state (OS) from XANES analysis are also given.

Initially, the Ir atoms are surrounded by four light atoms (N/C/O) and the valence state is +3.2 (Table 1), which is similar to Ir³⁺ in iridium (III) porphyrin and phthalocyanine complexes.^{48–50} During the pre-treatment under H₂ gas at 250°C, the coordination number reduces from 4.0 (\pm 0.1) to 2.9 (\pm 0.1), as illustrated in Figure 5A. This three-fold configuration has been already reported

for Cu, Mn and Co single atom catalysts supported on carbon nitride based materials,^{51–53} as well as Ir (II) complexes $(^R\text{N}_4)\text{Ir}(\text{COD})^{2+}$, where Ir was found to be coordinated with three nitrogen atoms.⁵⁴ Moreover, Fang *et al.*³⁵ found that Pt in Pt₁/N-C SAC shows a diminution of the coordination number (from 4 to 2) and the oxidation state (from + 1.89 to + 1.12) under electroreduction conditions, as evidenced by *operando* XAS.³⁵ The authors hypothesized that the high catalytic activity of the electrochemical hydrogen evolution reaction was mainly due to this evolution of the electronic properties and of the local arrangement of the atoms.

The coordination number reduction is accompanied by the decrease of the $R_{\text{Ir-X}}$ distance from 2.016 to 1.996 Å (Figure 5B) during the pre-treatment. A first explanation would be that the de-coordination allows a stronger interaction between the remaining neighbours and therefore smaller $R_{\text{Ir-X}}$ distances as for C-C bond whose length is reduced from 1.54 Å to 1.34 Å and 1.20 Å for the single, double and triple C-C bond respectively. A second explanation is based on the de-coordination of one longer Ir-X distance amongst the initial four neighbouring atoms. Previous literature reported smaller bond lengths of M-N as compared to M-O in metal SACs. For example, the distances Cu-N and Cu-O were found to be 1.91 Å and 2.01 Å, respectively, in a Cu SAC supported on carbon.⁵⁵ In a ZnN_x/C catalysts, the distances Zn-N and Zn-O are 2.00 Å and 2.14 Å, respectively.¹⁵ Furthermore, the Ir-N bond length in an Iridium Pincer complex, $(\text{NCN})\text{Ir}(\text{CH}_2\text{CH}_3)\text{Cl}(\text{OH}_2)$, is 2.051 Å which is significantly shorter than 2.259 Å for Ir-O.⁵⁶ Therefore, we hypothesize that $R_{\text{Ir-N}}$ is lower than $R_{\text{Ir-O}}$ in Ir-SAC supported on nitrogen doped carbon and consequently, this catalyst might lose one oxygen neighbour under reductive atmosphere.

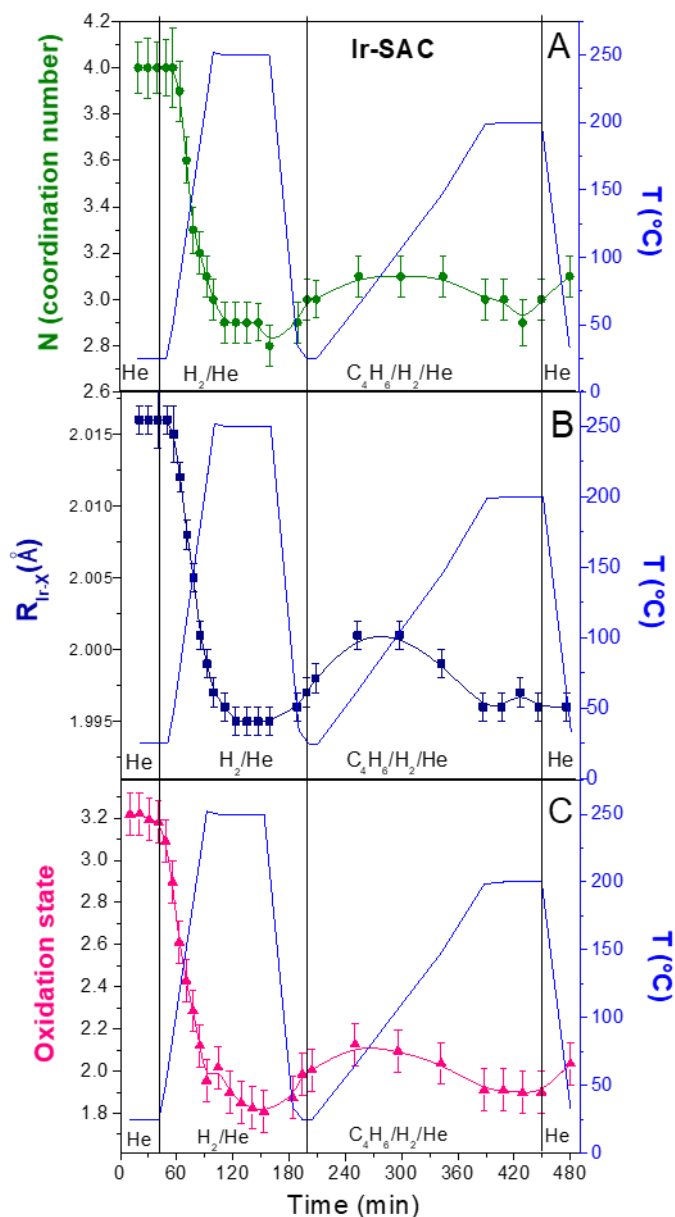


Figure 5. Variation of coordination number (A), the nearest neighbour distance Ir-X with X = C, N or O (B) and the Ir oxidation state (C) of Ir-SAC in operando conditions.

Assuming that the initial configuration is Ir-N_xC_yO_z (x + y + z = 4), we hypothesize that it evolves to Ir-N_xC_yO_z (x + y + z = 3) during the reduction pre-treatment. Moreover, a diminution of the oxidation state from +3.2 to +2.0 is also noticed during pre-treatment pointing out to a partial reduction under these conditions (Figure 5C). Therefore, these three parameters (coordination

number, R_{Ir-X} and oxidation state) are varying concomitantly pointing out that the reduction pre-treatment might imply the loss of one nearest neighbour around Ir atoms (possibly oxygen) accompanied by a decrease of both the average distance R_{Ir-X} and the oxidation state.

The coordination number, the R_{Ir-X} distance and the oxidation state slightly increase with the introduction of the reactive gas mixture at 25 °C. They continue to slightly raise during the temperature ramp up to around 80 °C which might be an artefact due to the gradual arrival of butadiene in the reactor. This is followed by a smooth decrease at higher temperature up to 200 °C that might be the evidence of the adsorption of carbonaceous reactants and products in the vicinity of Ir single-atoms. The decrease at high temperature is consistent with a classical decrease of the reactant/products surface coverage when the temperature increases. At steady reactive conditions at 200 °C and during cooling to 25 °C, these three parameters are stable, within the error bar proving that Ir SAC is exceptionally stable during the hydrogenation reaction.

It is interestingly to notice the matching evolutions of the coordination number, the nearest neighbour distance, and the oxidation state, irrespective of the gaseous environment and temperature. This is surprising since these values are extracted from different parts of the XAS spectrum: the coordination number and the nearest neighbour distance are determined from the EXAFS fitting requiring a structure input and the oxidation state is calculated from the XANES data without structural model. This relationship among two different sets of data confirms our robust data treatment and supports our following conclusion: Ir atoms surrounded by three light elements (N, C, O) are the main reactive species in the hydrogenation of butadiene.

It is obvious from these experiments that the geometric and the electronic state of the as-prepared Ir-SAC is different from the pre-treated (before reaction) and final (after reaction) states. This variation is mainly reflected by the reduction of the intensity of both the white line in the XANES spectra and the Fourier Transform modulus of the k^2 -weighed EXAFS signals from the initial state to the catalyst before and after reaction (Figure 6). Moreover, it is important to notice that Ir-SAC is stable during reaction without coalescence and formation of metallic aggregates since no additional peak at 2.6 Å (typical for Ir-Ir nearest distance) is observed after reaction (Figure 6B). The outstanding thermal stability of Ir single atoms will be addressed separately in a next paragraph.

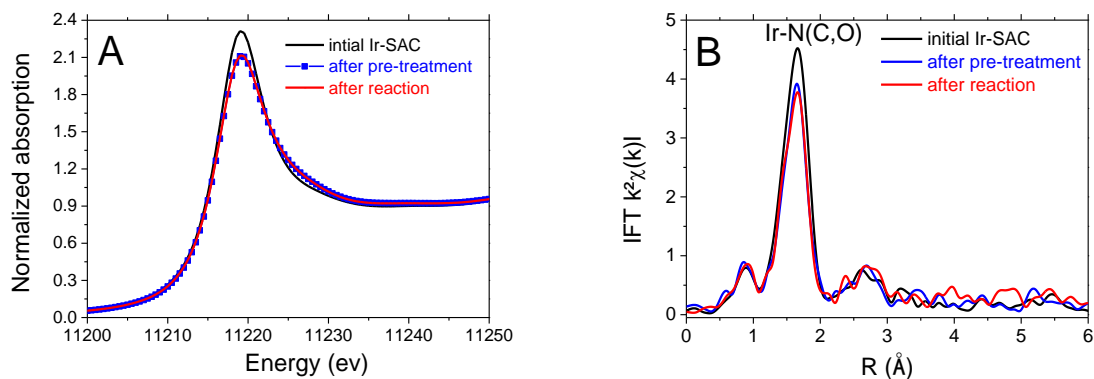


Figure 6. XANES spectra at the Ir L_3 -edge (A) and the modulus of the Fourier transforms of the k^2 -weighted EXAFS signals (B) of the Ir-SAC initial (black), after pre-treatment under H_2/He flow (blue) and after reaction (red) at room temperature.

For the sake of comparison, we have also performed *operando* XAS experiments on the Ir-NC sample. The Ir nanocatalyst is stable during the pre-treatment and reaction without any local structural or electronic change, irrespective of gaseous environment and temperature. The coordination number ($N = 9 \pm 1$) and the oxidation state (around 0) are constant during the pre-treatment and reaction. As expected, a small thermal variation can be noticed for the nearest neighbour distance: R_{Ir-Ir} increases from $2.710 \pm 0.009 \text{ \AA}$ to $2.720 \pm 0.009 \text{ \AA}$ while heating from $25 \text{ }^\circ\text{C}$ to $250 \text{ }^\circ\text{C}$, although this change is within the error bar. The Debye-Waller factor, σ^2 , raises likely from $0.0043 \pm 0.0005 \text{ \AA}^2$ to $0.0064 \pm 0.0005 \text{ \AA}^2$ during the temperature increase from $25 \text{ }^\circ\text{C}$ to $250 \text{ }^\circ\text{C}$. Moreover, no significant change of Ir-NC could be noticed when introducing the reactive gas mixture as well as during reaction. Selected XANES, EXAFS spectra and corresponding fits for Ir-NC are displayed in Figure SI4.

The gaseous product distributions during *operando* XAS experiments of both Ir-SAC and Ir-NC were detected by mass spectroscopy (Figure SI5). Ir-SAC is highly active and selective to butene isomers while butane is the principal product for Ir-NC. The result is consistent with laboratory catalytic tests, confirming that *operando* XAS experiments were conducted in real working conditions.

To further confirm the thermal stability of Ir-SAC, we have carried out *ex situ* STEM-HAADF imaging on the Ir-SAC powder treated under $5\%H_2/Ar$ flow at $250 \text{ }^\circ\text{C}$ and $400 \text{ }^\circ\text{C}$. Figure SI6 clearly

shows isolated bright spots homogeneously dispersed on the support, irrespective of the temperature. This confirms that Ir single atoms are stable after the thermal treatment under reducing gas, even at 400 °C. This result is particularly meaningful since the stability of single-atoms toward coalescence is a real issue, especially in reducing atmosphere⁵⁷. A thorough catalytic study complemented by detailed physicochemical characterizations will be addressed in a future report.

4. Conclusion

We have prepared Ir single atoms well dispersed on a nitrogen-doped carbon support and carried out catalytic tests for the partial hydrogenation of butadiene. The Ir-SAC proves a substantial activity toward hydrogenation of butadiene with nearly 100% selectivity to butenes even at full conversion. In comparison, Ir nanoparticles dispersed on a carbon support behave differently with low selectivity to butenes while the conversion exceeds 30%. By means of *operando* XAS experiments, we demonstrated that the reduction pre-treatment under H₂ at 250 °C involves the loss of one nearest neighbour (possibly oxygen) around Ir atoms accompanied by a decrease of the R_{Ir-X} distance as well as the oxidation state from +3.2 to +2.0. This evolution of the electronic and atomic structure of Ir-SAC might be the reason for the high catalytic selectivity in the hydrogenation of butadiene uncovering that the active species are Ir atoms surrounded by three light elements (N, C, O). Moreover, the Ir single atoms are stable at high temperature (up to 400 °C) without any coalescence into metallic clusters or nanoparticles. These results are of paramount importance for in-depth understanding of the underlying reaction mechanisms in the fast-growing field of the single-atom catalysis.

5. Acknowledgments

Fabrice Couturas and Stéphanie Belin are acknowledged for help during the XAS experiments on ROCK beam line at Soleil. WL and CZ would like to thank Julie Bourgon for TEM measurements. The authors acknowledge the French National Research Agency (ANR) for financial support (contract Ultracat ANR-17-CE06-0008-02). This work was supported by a public grant overseen by

the French National Research Agency (ANR) as part of the “Investissements d’Avenir” program (reference: ANR10-EQPX45).

6. References

- 1 Z. Li, S. Ji, Y. Liu, X. Cao, S. Tian, Y. Chen, Z. Niu and Y. Li, *Chem. Rev.*, 2020, **120**, 623–682.
- 2 C. M. Friend and B. Xu, *Acc. Chem. Res.*, 2017, **50**, 517–521.
- 3 X.-F. Yang, A. Wang, B. Qiao, J. Li, J. Liu and T. Zhang, *Acc. Chem. Res.*, 2013, **46**, 1740–1748.
- 4 X. Li, X. Yang, J. Zhang, Y. Huang and B. Liu, *ACS Catal.*, 2019, **9**, 2521–2531.
- 5 J. Liu, *ACS Catal.*, 2017, **7**, 34–59.
- 6 C. Rivera-Cárcamo and P. Serp, *ChemCatChem*, 2018, **10**, 5058–5091.
- 7 M. B. Gawande, P. Fornasiero and R. Zbořil, *ACS Catal.*, 2020, **10**, 2231–2259.
- 8 W. Zang, Z. Kou, S. J. Pennycook and J. Wang, *Adv. Energy Mater.*, 2020, 1903181.
- 9 J. Liu, *Current Opinion in Green and Sustainable Chemistry*, 2020, **22**, 54–64.
- 10 S. Mitchell, E. Vorobyeva and J. Pérez-Ramírez, *Angewandte Chemie International Edition*, 2018, **57**, 15316–15329.
- 11 N. Cheng, L. Zhang, K. Doyle-Davis and X. Sun, *Electrochem. Energ. Rev.*, 2019, **2**, 539–573.
- 12 B. Qiao, A. Wang, X. Yang, L. F. Allard, Z. Jiang, Y. Cui, J. Liu, J. Li and T. Zhang, *Nature Chemistry*, 2011, **3**, 634–641.
- 13 H. B. Yang, S.-F. Hung, S. Liu, K. Yuan, S. Miao, L. Zhang, X. Huang, H.-Y. Wang, W. Cai, R. Chen, J. Gao, X. Yang, W. Chen, Y. Huang, H. M. Chen, C. M. Li, T. Zhang and B. Liu, *Nat Energy*, 2018, **3**, 140–147.
- 14 M.-M. Millet, G. Algara-Siller, S. Wrabetz, A. Mazheika, F. Girgsdies, D. Teschner, F. Seitz, A. Tarasov, S. V. Levchenko, R. Schlögl and E. Frei, *J. Am. Chem. Soc.*, 2019, **141**, 2451–2461.
- 15 P. Song, M. Luo, X. Liu, W. Xing, W. Xu, Z. Jiang and L. Gu, *Advanced Functional Materials*, 2017, **27**, 1700802.
- 16 J. Gu, C.-S. Hsu, L. Bai, H. M. Chen and X. Hu, *Science*, 2019, **364**, 1091–1094.
- 17 G. Lei, Y. Tong, L. Shen, F. Liu, Y. Xiao, W. Lin, Y. Zhang, C. Au and L. Jiang, *Small*, 2020, **16**, 2003904.
- 18 W. Xiong, H. Li, H. Wang, J. Yi, H. You, S. Zhang, Y. Hou, M. Cao, T. Zhang and R. Cao, *Small*, 2020, **16**, 2003943.
- 19 X. Wang, L. Li, Z. Fang, Y. Zhang, J. Ni, B. Lin, L. Zheng, C. Au and L. Jiang, *ACS Catal.*, 2020, **10**, 9504–9514.
- 20 F. Hu, L. Leng, M. Zhang, W. Chen, Y. Yu, J. Wang, J. H. Horton and Z. Li, *ACS Appl. Mater. Interfaces*, 2020, **12**, 54146–54154.
- 21 M. L. Derrien, in *Studies in Surface Science and Catalysis*, ed. L. Cerveny, Elsevier, 1986, vol. 27, 613–666.
- 22 Q. Yang, R. Qiu, X. Ma, R. Hou and K. Sun, *Catal. Sci. Technol.*, 2020, **10**, 3670–3680.
- 23 S. Liu, S. Tan, B. Bian, H. Yu, Q. Wu, Z. Liu, F. Yu, L. Li, S. Yu, X. Song and Z. Song, *RSC Adv.*, 2018, **8**, 19551–19559.
- 24 F. J. Méndez, L. Piccolo, R. Solano, M. Aouine, Y. Villasana, J. Guerra, S. Curbelo, C. Olivera-Fuentes and J. L. Brito, *New J. Chem.*, 2018, **42**, 11165–11173.
- 25 T. Ouchaib, J. Massardier and A. Renouprez, *Journal of Catalysis*, 1989, **119**, 517–520.

- 26B. K. Furlong, J. W. Hightower, T. Y.-L. Chan, A. Sarkany and L. Gucci, *Applied Catalysis A: General*, 1994, **117**, 41–51.
- 27A. Sarkany, Z. Zsoldos, G. Stefler, J. W. Hightower and L. Gucci, *Journal of Catalysis*, 1995, **157**, 179–189.
- 28J. Goetz, M. A. Volpe, C. E. Gigola and R. Touroude, *Journal of Catalysis*, 2001, **199**, 338–345.
- 29Á. Molnár, A. Sárkány and M. Varga, *Journal of Molecular Catalysis A: Chemical*, 2001, **173**, 185–221.
- 30Z. Wang. "Selective Hydrogenation of Butadiene over Non-noble Bimetallic Catalysts". Material chemistry. Université Pierre et Marie Curie - Paris VI, 2017. English. NNT : 2017PA066102. tel-01825025.
- 31F. R. Lucci, J. Liu, M. D. Marcinkowski, M. Yang, L. F. Allard, M. Flytzani-Stephanopoulos and E. C. H. Sykes, *Nature Communications*, 2015, **6**, 8550.
- 32C.-Q. Lv, J.-H. Liu, Y. Guo and G.-C. Wang, *Applied Surface Science*, 2019, **466**, 946–955.
- 33H. Yan, H. Cheng, H. Yi, Y. Lin, T. Yao, C. Wang, J. Li, S. Wei and J. Lu, *J. Am. Chem. Soc.*, 2015, **137**, 10484–10487.
- 34X. Zhang, H. Shi and B.-Q. Xu, *Angew. Chem. Int. Ed.*, 2005, **44**, 7132–7135.
- 35S. Fang, X. Zhu, X. Liu, J. Gu, W. Liu, D. Wang, W. Zhang, Y. Lin, J. Lu, S. Wei, Y. Li and T. Yao, *Nat Commun*, 2020, **11**, 1029.
- 36L. Zhao, Y. Zhang, L.-B. Huang, X.-Z. Liu, Q.-H. Zhang, C. He, Z.-Y. Wu, L.-J. Zhang, J. Wu, W. Yang, L. Gu, J.-S. Hu and L.-J. Wan, *Nature Communications*, 2019, **10**, 1278.
- 37A. Malouche, Y. Oumellal, C. M. Ghimbeu, A. M. de Yuso and C. Zlotea, *J Nanopart Res*, 2017, **19**, 270.
- 38V. Briois, C. L. Fontaine, S. Belin, L. Barthe, T. Moreno, V. Pinty, A. Carcy, R. Girardot and E. Fonda, *J. Phys.: Conf. Ser.*, 2016, **712**, 012149.
- 39A. Michalowicz, J. Moscovici, D. Muller-Bouvet and K. Provost, *Journal of Physics: Conference Series*, 2009, **190**, 012034.
- 40A. Michalowicz, J. Moscovici, D. Muller-Bouvet and K. Provost, *Journal of Physics: Conference Series*, 2013, **430**, 012016.
- 41A. Malouche, G. Blanita, D. Lupu, J. Bourgon, J. Nelayah and C. Zlotea, *Journal of Materials Chemistry A*, 2017, **5**, 23043–23052.
- 42F. Morfin, S. Nassreddine, J. L. Rousset and L. Piccolo, *ACS Catal.*, 2012, **2**, 2161–2168.
- 43V. Monteseuro, J. A. Sans, V. Cuartero, F. Cova, I. A. Abrikosov, W. Olovsson, C. Popescu, S. Pascarelli, G. Garbarino, H. J. M. Jönsson, T. Irifune and D. Errandonea, *Sci Rep*, 2019, **9**, 8940.
- 44M. D. Hall, G. J. Foran, M. Zhang, P. J. Beale and T. W. Hambley, *J. Am. Chem. Soc.*, 2003, **125**, 7524–7525.
- 45H. Sun and W. Zhou, *Energy Fuels*, 2021, **35**, 5716–5737.
- 46Z. Li, Y. Chen, S. Ji, Y. Tang, W. Chen, A. Li, J. Zhao, Y. Xiong, Y. Wu, Y. Gong, T. Yao, W. Liu, L. Zheng, J. Dong, Y. Wang, Z. Zhuang, W. Xing, C.-T. He, C. Peng, W.-C. Cheong, Q. Li, M. Zhang, Z. Chen, N. Fu, X. Gao, W. Zhu, J. Wan, J. Zhang, L. Gu, S. Wei, P. Hu, J. Luo, J. Li, C. Chen, Q. Peng, X. Duan, Y. Huang, X.-M. Chen, D. Wang and Y. Li, *Nat. Chem.*, 2020, **12**, 764.
- 47Z. Chen, M. Xiao, J. Zhu, G. Li, N. Li, S. Li, Z. P. Cano, L. Ma, P. X. Cui, P. Xu, G. Jiang, H. Jin, S. Wang, T. Wu, J. Lu, A. Yu and D. Su, *Angew. Chem.*, 2019, **58**, 9640–9645.
- 48M. C. R. Castro, N. B. Sedrine, T. Monteiro and A. V. Machado, *Spectrochimica Acta Part A: Molecular and Biomolecular Spectroscopy*, 2020, **235**, 118309.

- 49 H. Cui, Y. Wang, Y. Wang, Y.-Z. Fan, L. Zhang and C.-Y. Su, *CrystEngComm*, 2016, **18**, 2203–2209.
- 50 K. Murata and K. Ishii, *Eur. J. Inorg. Chem.*, 2017, **2017**, 5103–5107.
- 51 P. Yang, S. Zuo, F. Zhang, B. Yu, S. Guo, X. Yu, Y. Zhao, J. Zhang and Z. Liu, *Ind. Eng. Chem. Res.*, 2020, **59**, 7327–7335.
- 52 W. Liu, W. Hu, L. Yang and J. Liu, *Nano Energy*, 2020, **73**, 104750.
- 53 J. Feng, H. Gao, L. Zheng, Z. Chen, S. Zeng, C. Jiang, H. Dong, L. Liu, S. Zhang and X. Zhang, *Nature Communications*, 2020, **11**, 4341.
- 54 K. Fuchigami, N. P. Rath and L. M. Mirica, *Inorg. Chem.*, 2017, **56**, 9404–9408.
- 55 Y. Cai, J. Fu, Y. Zhou, Y.-C. Chang, Q. Min, J.-J. Zhu, Y. Lin and W. Zhu, *Nature Communications*, 2021, **12**, 586.
- 56 L.A. Wingard PhD thesis *Accessing Intermediate and High Oxidation States with Tungsten and Iridium Pincer Complexes*. University of North Carolina at Chapel Hill, 2012.
- 57 C. Dessal, A. Sangnier, C. Chizallet, C. Dujardin, F. Morfin, J.-L. Rousset, M. Aouine, M. Bugnet, P. Afanasiev and L. Piccolo, *Nanoscale*, 2019, **11**, 6897–6904.